



## Multiple-photon transitions in electrically detected magnetic resonance measurements of 4H-SiC transistors

James P. Ashton \* and Patrick M. Lenahan

Department of Engineering Science and Mechanics, The Pennsylvania State University, University Park, Pennsylvania 16802, USA

 (Received 10 May 2020; revised 29 June 2020; accepted 30 June 2020; published 17 July 2020)

We report an ultralow-field frequency-swept electrically detected magnetic resonance (fsEDMR) measurement scheme sensitive to so-called ultrastrong coupling in paramagnetic systems, which arises from comparatively strong driving fields and weak Zeeman interaction with small static fields. We observe multiple-photon transitions in the EDMR spectrum of a 4H-SiC transistor. The multiphoton transitions are a strong function of the linearly polarized driving field and of the static field. The observation of both field-swept EDMR at a constant frequency and fsEDMR demonstrate that the transitions we observe are caused by multiphoton transitions. In the small static field and large driving-field regime, Bloch-Siegert effects cause small changes to the resonant frequency. We observe these Bloch-Siegert shifts in the resonance frequency in the ultralow-field fsEDMR scheme and verify the observation by also measuring the driving field directly using Faraday's law of induction and a sensing coil. Multiphoton transitions are important for quantum engineering applications.

DOI: [10.1103/PhysRevB.102.020101](https://doi.org/10.1103/PhysRevB.102.020101)

Multiple-photon transitions have been observed in nuclear magnetic resonance [1–3], electron paramagnetic resonance (EPR) [4,5], and in optically detected magnetic resonance [6]. The multiphoton transitions have widespread applicability from electrically driven magnetic resonance of spins in quantum dots [7], magnetic resonance imaging [8], and manipulation of coherent spin states in spin-based qubits used for quantum computation [9]. Furthermore, in the ultrastrong coupling regime, Bloch-Siegert shifts (BSS) emerge [10], which have applications in imaging [11] and quantum computing [12]. Both multiphoton transitions and BSS are observed in this work in the electrically detected magnetic resonance (EDMR) spectrum of interface defects in 4H-SiC/SiO<sub>2</sub> metal-oxide-semiconductor field-effect transistors (MOSFETs). The absorption of two or more photons requires conservation of angular momentum. Right and left circularly polarized photons have corresponding angular momentum  $J = 1$  with  $m_j = \pm 1$  denoted as  $\sigma^\pm$  photons, respectively. For multiphoton transitions, discrete numbers of photons are absorbed for the transitions. In the work of Clerjoud and Gelineau, the  $n = 2$  transition and  $n = 3$  transition were observed in conventional EPR, where  $n$  is the number of photons [4]. They account for the angular momentum conservation for the two-photon transition by labeling one of the absorbed quanta as a  $\pi$  photon which would exist if some component of the linearly polarized driving field ( $B_1$ ) was parallel with the static field  $B_0$ . The  $\pi$ -type photons are associated with  $m_j = 0$ ; these photons can be absorbed or emitted by the spin system regardless of the spin angular momentum difference of the transition since the wave function of the  $\pi$  photon is  $\pi = \frac{1}{\sqrt{2}}(\sigma^+ + \sigma^-)$  [5]. At ultralow magnetic fields ( $\leq 0.5$  mT) which would involve driving-field frequencies in the range of  $\sim 5$ –15 MHz or less, the electron spin Zeeman

interaction is small and comparable to  $B_1$ . Mkhitarian *et al.* show that, in weak field measurements, interaction of the spin system with the environment can cause the two-photon transition [4]. The effect of the environment can be viewed as a time-dependent tilt of the DC field [13]. Mkhitarian *et al.* modeled the environment for the two-photon absorption as a fluctuator coupled to the spin via the dipole interaction [13]. We utilize the model proposed by Mkhitarian *et al.* to analyze the shapes of the two-photon resonances [13]. We find strong agreement between the theory of Mkhitarian *et al.* [13] and our experimental results. Ultralow-field EDMR measurements of spin-dependent recombination currents in SiC devices provide a particularly convenient system to study the ultrastrong coupling regime ( $B_1 \approx B_0$ ). At such low fields and frequencies, the environment enabling the two-photon transition can be conveniently studied; in the case of 4H-SiC, the environment would be influenced by (small) hyperfine fields [13]. We observe the electrical detection of the two-photon transition utilizing both continuous-wave EDMR (cwEDMR) and frequency-swept (fs) EDMR. The observation of these transitions in both fsEDMR and cwEDMR demonstrates that they are certainly due to multiphoton transitions; it rules out the possibility of harmonic detection from the apparatus. Ultralow-field fsEDMR is a convenient scheme for studying the EDMR response within the sub-mT range because fsEDMR eliminates a near-zero field magnetoresistance (NZFMR) response, which often dominates the sub-mT regime in a magnetic field-swept measurement [14,15].

Continuous-wave EDMR is achieved in a manner much the same as EPR aside from the detection scheme. In EDMR, a change in device current occurs at resonance. To understand the EDMR results of this paper, we provide a brief discussion of EPR. Consider a sample with paramagnetic defects that is placed within a microwave cavity situated between the pole faces of an electromagnet. Consider first the simplest possible case in which unpaired electrons residing in these defects are

\*jamesashton1015@gmail.com

otherwise unperturbed by their local environment. The cavity along with a microwave bridge provides microwave radiation of energy  $E = h\nu$ , where  $h$  is Planck's constant and  $\nu$  is the microwave frequency. The electromagnet provides a magnetic field  $B$ ; its magnitude splits the unpaired electrons' energy via the Zeeman interaction. The energy of the electron spins in this  $B$  field is split into two levels characterized by the electrons' spin quantum number  $m_s$  which can either be  $+1/2$  or  $-1/2$ . When the microwave radiation energy is equal to the difference in energy between the electrons'  $+1/2$  and  $-1/2$  levels [16,17],  $h\nu = g_e\mu_B B$ , resonance occurs and the electrons transition from  $+1/2$  to  $-1/2$  (or vice versa). Here,  $g_e$  is the Landé  $g$  factor ( $g_e \approx 2.0023 \dots$ ),  $\mu_B$  is the Bohr magneton, and  $B$  is the magnitude of the applied field. In EPR, the absorption of microwave power is detected. Information about the defect's local environment is extracted via deviations to this resonance condition, two of which are spin-orbit coupling and electron-nuclear hyperfine interactions [16]. Electron-nuclear hyperfine interactions are the interactions between the magnetic moments of the unpaired electrons and the magnetic nuclei. EDMR is based on the intermediate coupling of two electrons which results in a nearly field and frequency independent sensitivity [18]. Thus, ultralow field EDMR measurements are possible without a loss in signal amplitude [18]. For the low magnetic fields utilized, spin-spin interactions are also important to understand our results [19,20].

One way in which EDMR takes place is through spin dependent recombination (SDR). SDR can be understood by theory first developed in a seminal paper by Kaplan, Solomon, and Mott [18]. Consider the following (qualitative) explanation of SDR. When a conduction electron encounters a deep level paramagnetic defect, the unpaired electron will couple with the conduction electron to form an intermediate state. If both electron spins are parallel, the electron will be unable to transition into the paramagnetic defect as this transition would violate the Pauli Exclusion Principle; these triplet states (spin angular momentum  $S = 1$ ) tend to dissociate. However, at resonance, spin flipping events at the deep level site will transform triplet states into singlet states (spin angular momentum  $S = 0$ ), in which the unpaired electron and conduction electron spins are anti-parallel. Now the conduction electron may fall into the deep level and will subsequently recombine with a valance band hole. (This sequence could be reversed with the hole capture followed by electron capture.) The singlet state transition and subsequent recombination conserves spin angular momentum, as  $S = 0$ , while triplet state capture and recombination will not, as  $S = 1$ . Other spin dependent transitions detected via EDMR are also possible, such as spin-dependent trap-assisted tunneling [19,21–23].

EPR observations of multiples of the resonance field corresponding to multiphoton transitions have been reported previously [4]. Quite recently, Mkhitarian *et al.* have addressed, in some detail, the theory of two-photon absorption in magnetic resonance [13]. They model the two-photon resonance line shape as a function of drive ( $B_1/B_0$ ) and show that for strong drive, the two-photon line shape is a single peak whose spectrum narrows with increasing drive. For weak drive, the two-photon line shape is a two-peaked line with a broader line shape. The ratio ( $B_1/B_0$ ) has also previously been explored in

studies of the transition amplitudes corresponding to multiphoton transitions [5]. For larger transition amplitudes, which are proportional to this ratio, the more likely the multiphoton transitions are to occur. Thus, we expect and observe that ultralow-field (sub-mT) EDMR measurements yield a high sensitivity to multiphoton transitions.

We utilize an n-channel 4H-SiC MOSFET with a thermal ONO oxide with thickness 50 nm. These samples have recently been utilized in SDR measurements [24]; they have a very large density of interface defects which yield a large EDMR response. Charge-pumping measurements [25–27] indicate that the average interface defect density is  $2 \times 10^{12} \text{ cm}^{-2} \text{ eV}^{-1}$ . The gate area is  $250 \times 20 \mu\text{m}^2$ . We utilize the bipolar amplification effect (BAE) measurement [28], which is an SDR measurement sensitive to 4H-SiC/SiO<sub>2</sub> interface traps with energy levels within the vicinity of the middle of the 4H-SiC band gap. In BAE, the MOSFET drain to body contact is forward biased well past the junction built-in voltage and the gate is biased close to but below inversion so that the electrons injected from the drain will travel at or very near to the 4H-SiC/SiO<sub>2</sub> interface as they proceed to the source. The body is grounded and the current is monitored through the source, which is held at virtual ground. Our experimental apparatus utilizes a custom-built electromagnet with built in modulation coils situated inside a three-layer cylindrical  $\mu$ -metal zero-Gauss chamber with outer shield 2.8 m long and 0.6 m in diameter. We utilize a Kepco BOP 20-5D bipolar power supply for magnet power, a Lake Shore Cryotronics 475 DSP Gaussmeter and Hall probe, a Stanford Research Systems SR570 preamplifier, a LABVIEW-based virtual lock-in amplifier, a Marconi/IFR 2026Q rf source fed into a custom-built resonator with diameter 6.6 mm with nine turns, a LeCroy LC564A 1 GHz oscilloscope for power monitoring, and a LABVIEW-based graphical user interface for magnetic-field modulation, data acquisition, magnetic-field control, and power leveling. Magnetic-field modulation is supplied from the computer, amplified by an Insignia stereo amplifier, and subsequently fed into the built-in modulation coils. Figure 1 illustrates a diagram of the experimental setup. For 87.5-MHz measurements, a Doty Scientific 85-MHz, 12-mm-diameter resonator coil was utilized with a 10-W HD Communications Corp. HD29347 1 – 1025-MHz rf amplifier. All measurements were performed at room temperature.

Sweeping frequency can result in changes in the rf level caused by the impedance of the resonator. These changes in rf level could significantly impact the AC device current detected causing power fluctuations in the device that distort the EDMR spectrum. This problem is circumvented by utilizing a proportional-integral-derivative (PID) controller to monitor the power level utilizing a GHz oscilloscope as mentioned previously. The PID scheme for power leveling has recently been introduced by Manning *et al.* for electrically detected electron nuclear double-resonance measurements [29]. The voltage out of the rf source is measured by a GHz oscilloscope and is fed back to the PID controller so that power-level changes are corrected.

Figure 2 illustrates the low-field/frequency (87.5-MHz) cwEDMR and NZFMR [14,15] spectrum for the 4H-SiC MOSFET sample. Here, we utilize the Doty Scientific resonator coil. In this measurement, magnetic-field modulation

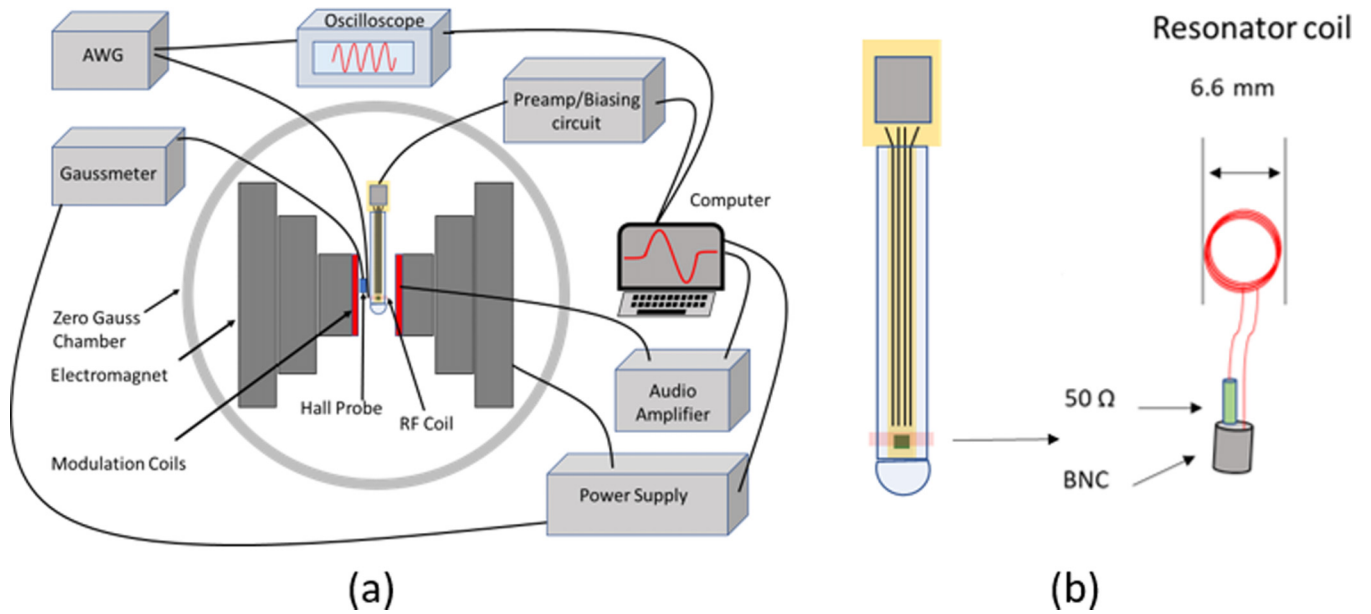


FIG. 1. (a) Schematic illustration of the experimental apparatus; (b) the custom-built resonator.

was utilized. From Fig. 2, the two-photon transition at  $B \approx 6$  mT is present. Here, the rf field  $B_1 \approx 0.11$  mT, which was measured utilizing a two-turn 12-mm-diameter (matched with the resonator) sensing coil. Thus, the ratio of  $B_1/B_0 \approx 10^{-2}$ . A half-field “forbidden”  $\Delta m_s = 2$  transition is present in Fig. 2, which involves the dipolar interaction of the unpaired electron spin to the conduction-level electron (The half-field transitions can be utilized to count the number of spins, or paramagnetic defects, in the sample [17,19,20].) The spectrum in Fig. 2 has side structures in the EDMR

response, which are separated by 1.1 mT. These side peaks are presumably the result of hydrogen complexed  $E'$  centers in the MOSFET gate oxide [30–33]. It should be noted that the defects studied here presumably have spin-spin relaxation times in the 10s of  $\mu$ s and spin-lattice relaxation times in the range of 100s of  $\mu$ s at room temperature based on recent literature [34–37].

As anticipated, the multiphoton transitions of the EDMR spectrum are much more pronounced at ultralow magnetic fields and rf frequencies. We have made measurements in the range of 0.2 – 0.5 mT corresponding to rf frequencies of 5.6 – 14 MHz. Since such low resonant fields are utilized, we have housed the low-field spectrometer inside of a zero-Gauss chamber. This eliminates stray magnetic fields caused by the various electronic components utilized and also eliminates the Earth’s ambient magnetic field ( $\approx 0.05$  mT). In the ultralow-field and frequency measurements, we utilize a second custom-built resonator with a 6.6-mm diameter as illustrated in Fig. 1. The values of  $B_1$  were again determined utilizing a diameter-matched 3-turn 6.6-mm sensing coil. Figure 3 shows representative field-swept EDMR spectra with the rf frequency held at 8.4 MHz for  $B_1 \approx 0.10$  mT,  $B_1 \approx 0.06$  mT, and  $B_1 \approx 0.03$  mT. Here, we utilize frequency modulation of the rf to eliminate the NZFMR response. It is clear from Fig. 3 that the  $n = 2$  transition can be observed for  $B_1 \approx 0.10$  mT and  $B_1 \approx 0.06$  mT. Note that signal to noise of the  $n = 2$  response for  $B_1 \approx 0.06$  mT limits our measure of the center crossing of this line. The line is presumably caused by the two-photon transition evident from the position of the peak (twice the resonant field). The transition disappears at lower power levels. In Fig. 4, we present fsEDMR measurements observed at static magnetic fields of 0.2, 0.3, 0.4, and 0.5 mT. In these measurements, the values of the driving field  $B_1 \approx 0.10$  mT,  $B_1 \approx 0.06$  mT,  $B_1 \approx 0.03$  mT,  $B_1 \approx 0.015$  mT. It is clear that with a decrease in  $B_0$  and an increase in  $B_1$ , peaks appear at  $\nu_n = \nu_0/n$  where  $\nu_0$  is the frequency at which the  $n = 1$  transition occurs (the classical

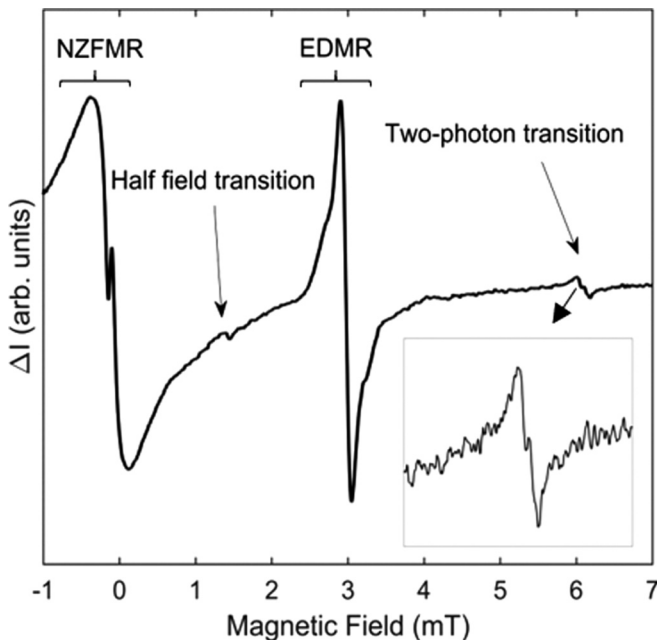


FIG. 2. NZFMR and low-field and -frequency (3 mT/87.5 MHz) cwEDMR spectrum for the 4H-SiC transistor. The inset shows the two-photon transition of the cwEDMR spectrum occurring at 6 mT.

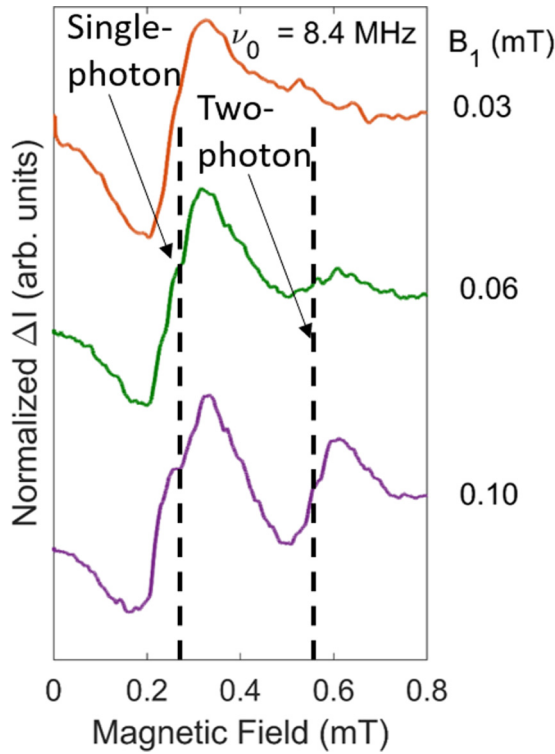


FIG. 3. Representative field-swept ultralow-field EDMR utilizing frequency modulation of the rf. The rf frequency was 8.4 MHz. Note that the two-photon transition is clearly present at twice the resonant field for  $B_1 \approx 0.06$  mT and  $B_1 \approx 0.10$  mT.

transition). It is quite obvious from this plot that the peaks occur at divisions of the rf frequency corresponding to integer  $n > 1$ . Table I provides a list of the peak positions and widths of each transition. This confirms that the observed double-field resonances in the cwEDMR measurements are the result of multiphoton transitions as this result could not be caused

by harmonics. If these transitions were harmonic detection of the source frequency, one would expect to observe the fsEDMR transitions at integer *multiples* of the resonance frequency. However, it is clear from Fig. 4 that this does not occur and we observe transitions at integer *divisions* of the rf frequency, consistent with multiphoton transitions [7]. The two-photon transition is a forbidden transition. However, as recently proposed by Mkhitarian *et al.* [13], the observation of the two-photon transition is a consequence of dipole coupling of the paramagnetic center with the environment which can be modeled as “noise.” In EDMR measurements of organic light-emitting diodes (OLED), the noise amplitude is controlled by local hyperfine fields [13,38]. In EDMR measurements of 4H-SiC MOSFETs, hyperfine fields would also control the level of noise. (It may be worth pointing out that, in 4H-SiC, the hyperfine fields could be controlled via isotopic substitution of  $^{12}\text{C}$  and  $^{28}\text{Si}$ .) Thus, one could effectively *tune* the environment with isotopic substitution; the two-photon transitions could be utilized to study this effect.

Mkhitarian *et al.* predicted that the shape of the two-photon transition for weak drive ( $B_1 \ll B_0$ ) should have a two-peak structure [13]. One can see this result in the two-photon curve of Fig. 2 at  $B \approx 6$  mT corresponding to weak drive since  $B_1/B_0 \approx 10^{-2}$ . In the fsEDMR spectra of Fig. 4, the two-photon transitions are single peaks whose linewidths narrow with increasing drive. This spectral narrowing of the two-photon line was also predicted by Mkhitarian *et al.* [13] for strong drive; the single-peak profile of the two-photon transition is sensitive to changes in  $B_1$  since the profile  $I(\beta) \propto 1/(1 + \beta^2\delta^2)$ , where  $\delta$  is a dimensionless quantity which incorporates the detuning from the two-photon resonance and  $\beta \propto B_1^4/B_0^4$  is a dimensionless quantity which incorporates the effect of drive [13]. From Fig. 4 and Table I, the width of the two-photon curve decreases with increasing  $B_1/B_0$  but is only weakly dependent, consistent with the conclusions of Mkhitarian *et al.* [13].

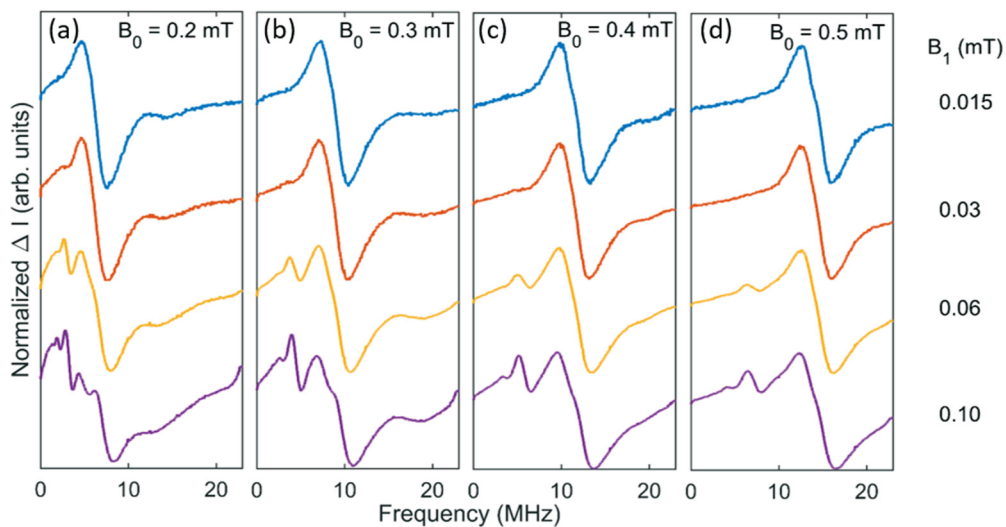


FIG. 4. Frequency-swept ultralow-field EDMR. The amplitudes have been normalized. (a)  $B_0$  set to 0.2 mT, (b)  $B_0$  set to 0.3 mT, (c)  $B_0$  set to 0.4 mT, and (d)  $B_0$  set to 0.5 mT. It is clear that the multiphoton transitions are dependent on both  $B_0$  and  $B_1$ . The multiphoton transitions occur at integer divisions of the rf resonant frequency. The  $n = 3$  transition is observed for  $B_1$  at 0.10 mT and  $B_0$  at 0.2 mT. The  $n = 2$  transition is observed for  $B_1 \geq 0.06$  mT.

TABLE I. Positions  $f$  and width  $w$  (in units of MHz) of the single- ( $n = 1$ ), two- ( $n = 2$ ), and three- ( $n = 3$ ) photon transition from Fig. 4 for  $B_1 \geq 0.06$  mT.

$B_1 \backslash B_0$	0.2 mT	0.3 mT	0.4 mT	0.5 mT
$\approx 0.10$ mT	$n = 1 : f = 6.3$ $w = 4.0$ $n = 2 : f = 3.2$ $w = 0.8$ $n = 3 : f = 2.1$ $w = 0.4$	$n = 1 : f = 8.8$ $w = 4.3$ $n = 2 : f = 4.4$ $w = 1.0$	$n = 1 : f = 11.4$ $w = 4.2$ $n = 2, f = 5.8$ $w = 1.4$	$n = 1 : f = 14.1$ $w = 4.3$ $n = 2 : f = 7.1$ $w = 1.5$
$\approx 0.06$ mT	$n = 1 : f = 6.1$ $w = 3.4$ $n = 2 : f = 3.0$ $w = 0.9$	$n = 1 : f = 8.6$ $w = 3.7$ $n = 2 : f = 4.3$ $w = 1.2$	$n = 1, f = 11.4$ $w = 3.8$ $n = 2, f = 5.7$ $w = 1.5$	$n = 1, f = 14.1$ $w = 3.6$ $n = 2, f = 7.0$ $w = 1.6$

We expect to observe the BSS [10] of the rf frequency, which occurs for a strong linearly polarized  $B_1$  when  $B_0$  is weak. According to Clerjaud and Gelineau, for odd transitions, the shift in frequency caused by the Bloch-Siegert effect is [4]

$$\Delta v = \left[ \frac{(\gamma B_1)^2}{4v} \right], \quad p = 0, \quad \text{and}$$

$$\Delta v = \left[ \frac{(\gamma B_1)^2}{4v} \right] (2p + 1)/p(p + 1), \quad p = 1, 2, 3, \dots \quad (1)$$

Here,  $\gamma$  is the gyromagnetic ratio for the electron (28 MHz/mT),  $n = 2p + 1$  is the number of photons for the given transition, and  $v$  is the rf frequency. Equation (1) can provide a first-order estimate of the rf field  $B_1$  [4,39]. For the  $n = 1, p = 0$  transition, we calculate  $B_1$  from the BSS corresponding to the sensing coil measurement of  $B_1 \approx 0.10$  mT and  $B_1 \approx 0.06$  mT (at lower  $B_1$ , the shift is on the order of a few hundredths of a MHz which is below our detection limit). The results are shown in Table II.

The error between the BSS  $B_1$  and the  $B_1$  estimated with the sensing coil is mainly caused by the error in the frequency measurement of the center crossing of the spectra (signal-to-noise limitation) and, to a lesser extent, error of the sensing coil measurement. The  $B_1$  values between the two measurements fall within range of one another. We thus conclude that the BSS extracted  $B_1$  is in agreement with  $B_1$  measured via the sensing coil. We have confirmed the extraction of BSS  $B_1 \approx 0.12$  mT via the BSS for the spectrum of Fig. 4 corresponding to  $B_0 \approx 0.3$  mT and  $B_1 \approx 0.10$  mT measured via the sensing coil [Fig. 5(b), bottom spectrum]. The utilization of BSS for determination of  $B_1$  has been reported elsewhere [8,11,39]. This is an observation of BSS in an EDMR measurement.

In conclusion, we present ultralow-field fsEDMR and magnetic-field-swept cwEDMR results that directly measure multiphoton transitions of the EDMR spectrum of 4H-SiC/SiO<sub>2</sub> interface defects in 4H-SiC MOSFETs. For the ultralow-field range explored here (0.2–0.5 mT), a cwEDMR measurement utilizing conventional magnetic-field modulation would be impossible as a NZFMR response would overwhelm most, if not all, of the ultralow-field EDMR spectrum. We are able to circumvent this problem by utilizing frequency modulation of the rf field. We provide representative cwEDMR spectra as a function of the driving field  $B_1$  and show that transitions corresponding to multiphoton absorption occur at multiples of the rf resonance field. We also utilize fsEDMR at ultralow magnetic fields to confirm the observed multiphoton transitions. In the fsEDMR measurements, we are able to observe transitions up to  $n = 3$  photons (Fig. 4). In addition, we observe Bloch-Siegert shifting of the EDMR frequency in our fsEDMR measurements which we confirm via direct measurement of  $B_1$  via Faraday’s law with a sensing coil. This represents EDMR observation of the multiphoton transitions in an inorganic semiconductor device. The multiphoton transitions and Bloch-Siegert effect are both important for quantum engineering applications, such as spin-based quantum computation.

We would like to thank Brian R. Manning for his contributions to the spectrometer setup and automatic power leveling. We would also like to thank Stephen J. Moxim for acquiring data and fruitful discussions regarding the interpretation of the results. This work at Penn State was supported by the US Army Research Laboratory. Any opinions, findings, conclusions, or other recommendations expressed herein are those of the authors and do not necessarily reflect the views of the US Army Research Laboratory. This work was also supported by the Air Force Office of Scientific Research under Award No. FA9550-17-1-0242.

TABLE II. Bloch-Siegert shift in MHz,  $B_1$  measured with a sensing coil, and  $B_1$  extracted from (1) for the spectra of Fig. 4(a).

Approximate BSS $\Delta v$ (MHz)	$B_1$ estimated with the sensing coil (mT)	$B_1$ measured through the BSS (mT)
0.5	$0.10 \pm 0.01$	$0.12 \pm 0.03$
0.2	$0.06 \pm 0.01$	$0.08 \pm 0.04$

- [1] S. Yatsiv, *Phys. Rev.* **113**, 1522 (1959).
- [2] Y. Zur, M. H. Levitt, and S. Vega, *J. Chem. Phys.* **78**, 5293 (1983).
- [3] P. Bucci, P. Cavaliere, and S. Santucci, *J. Chem. Phys.* **52**, 4041 (1970).
- [4] B. Clerjoud and A. Gelineau, *Phys. Rev. Lett.* **48**, 40 (1982).
- [5] J. Dolinšek, M. Vilfan, and S. Žumer, *Novel NMR and EPR Techniques* (Springer, Berlin, 2006).
- [6] V. A. Morozov, A. V. Antzutkin, A. V. Koptug, and A. B. Doktorov, *Mol. Phys.* **73**, 517 (1991).
- [7] J. Romhányi, G. Burkard, and A. Pályi, *Phys. Rev. B* **92**, 054422 (2015).
- [8] V. Han and C. Liu, *Magn. Reson. Med.* **84**, 1184 (2020).
- [9] S. Bertaina, L. Chen, N. Groll, J. Van Tol, N. S. Dalal, and I. Chiorescu, *Phys. Rev. Lett.* **102**, 050501 (2009).
- [10] F. Bloch and A. Siegert, *Phys. Rev.* **57**, 522 (1940).
- [11] L. I. Sacolick, F. Wiesinger, I. Hancu, and M. W. Vogel, *Magn. Reson. Med.* **63**, 1315 (2010).
- [12] P. Forn-Díaz, J. Lisenfeld, D. Marcos, J. J. García-Ripoll, E. Solano, C. J. P. M. Harmans, and J. E. Mooij, *Phys. Rev. Lett.* **105**, 237001 (2010).
- [13] V. V. Mkhitaryan, C. Boehme, J. M. Lupton, and M. E. Raikh, *Phys. Rev. B* **100**, 214205 (2019).
- [14] C. J. Cochrane and P. M. Lenahan, *J. Appl. Phys.* **112**, 123714 (2012).
- [15] J. P. Ashton, S. J. Moxim, P. M. Lenahan, C. G. McKay, R. J. Waskiewicz, K. J. Myers, M. E. Flatte, N. J. Harmon, and C. D. Young, *IEEE Trans. Nucl. Sci.* **66**, 428 (2019).
- [16] W. Gordy, *Theory and Applications of Electron Spin Resonance* (John Wiley & Sons, New York, 1980).
- [17] C. P. Slichter, *Principles of Magnetic Resonance*, 3rd ed. (Springer-Verlag, Berlin, 1978).
- [18] D. Kaplan, I. Solomon, and N. F. Mott, *J. Phys. Lett.* **39**, 51 (1978).
- [19] C. J. Cochrane and P. M. Lenahan, *Appl. Phys. Lett.* **104**, 093503 (2014).
- [20] S. S. Eaton, K. M. More, B. M. Sawant, and G. R. Eaton, *J. Am. Chem. Soc.* **105**, 6560 (1983).
- [21] M. A. Anders, P. M. Lenahan, C. J. Cochrane, and J. Van Tol, *J. Appl. Phys.* **124**, 215105 (2018).
- [22] M. J. Mutch, P. M. Lenahan, and S. W. King, *Appl. Phys. Lett.* **109**, 062403 (2016).
- [23] R. J. Waskiewicz, M. J. Mutch, P. M. Lenahan, and S. W. King, in *2016 IEEE International Integrated Reliability Workshop (IIRW)* (IEEE, New York, 2016), pp. 99–102.
- [24] J. P. Ashton, P. M. Lenahan, D. J. Lichtenwalner, A. J. Lelis, and M. A. Anders, *J. Appl. Phys.* **126**, 145702 (2019).
- [25] A. B. M. Elliot, *Solid State Electron.* **19**, 241 (1976).
- [26] S. J. Brugler and P. G. Jespers, *IEEE Trans. Electron Devices* **ED-16**, 297 (1969).
- [27] G. Groeseneken, H. E. Maes, N. Beltran, and R. F. D. E. Keersmaecker, *IEEE Trans. Electron Devices* **ED-31**, 42 (1984).
- [28] T. Aichinger and P. M. Lenahan, *Appl. Phys. Lett.* **101**, 083504 (2012).
- [29] B. R. Manning, R. J. Waskiewicz, D. J. McCrory, and P. M. Lenahan, *Rev. Sci. Instrum.* **90**, 123111 (2019).
- [30] C. J. Cochrane, P. M. Lenahan, and A. J. Lelis, *J. Appl. Phys.* **109**, 014506 (2011).
- [31] P. M. Lenahan, C. Cochrane, and A. Lelis, *ECS Trans.* **64**, 111 (2014).
- [32] M. A. Anders, P. M. Lenahan, C. J. Cochrane, and A. J. Lelis, *IEEE Trans. Electron Devices* **62**, 301 (2015).
- [33] M. A. Anders, P. M. Lenahan, and A. J. Lelis, *J. Appl. Phys.* **122**, 234503 (2017).
- [34] S. G. Carter, O. O. Soykal, P. Dev, S. E. Economou, and E. R. Glaser, *Phys. Rev. B* **92**, 161202(R) (2015).
- [35] R. Nagy, M. Niethammer, M. Widmann, Y. C. Chen, P. Udvarhelyi, C. Bonato, J. U. Hassan, R. Karhu, I. G. Ivanov, N. T. Son, J. R. Maze, T. Ohshima, Ö. O. Soykal, Á. Gali, S. Y. Lee, F. Kaiser, and J. Wrachtrup, *Nat. Commun.* **10**, 1954 (2019).
- [36] C. Kasper, D. Klenkert, Z. Shang, D. Simin, A. Gottscholl, A. Sperlich, H. Kraus, C. Schneider, S. Zhou, M. Trupke, W. Kada, T. Ohshima, V. Dyakonov, and G. V. Astakhov, *Phys. Rev. Appl.* **13**, 044054 (2020).
- [37] A. J. Ramsay and A. Rossi, *Phys. Rev. B* **101**, 165307 (2020).
- [38] D. P. Waters, G. Joshi, M. Kavand, M. E. Limes, H. Malissa, P. L. Burn, J. M. Lupton, and C. Boehme, *Nat. Phys.* **11**, 910 (2015).
- [39] I. Hung, P. Gor'kov, and Z. Gan, *J. Magn. Reson.* **310**, 106636 (2020).